An Experimental Study of the Water Transfer Through Confined Compacted GMZ Bentonite

Wei-Min Ye, Yu-Jun Cui, Li-Xin Qian, Bao Chen

An Experimental Study of the Water Transfer Through Confined Compacted GMZ Bentonite

W.M. Ye [1], Y.J. Cui [2*], L.X. Qian [1,2], B. Chen [1]

1: Tongji University, 1239 Siping Road, 200092 Shanghai, P. R. of China
2: Ecole des Ponts-ParisTech, UR Navier-CERMES, 6 et 8 avenue Blaise Pascal, Cité Descartes, Champs-sur-Marne, 77455 Marne-la-Vallée cedex 2, France (cui@cermes.enpc.fr)

* Corresponding author

Abstract:
GMZ bentonite has been considered as a possible material for engineered barrier in the Chinese program of nuclear waste disposal at great depth. In the present work, the hydraulic conductivity of this bentonite was determined by simultaneous profile method. A specific infiltration cell equipped with five resistive relative humidity probes was designed for this purpose. The water retention properties were studied under both confined and unconfined conditions; the results shows that at high suctions (> 4 MPa) the water retention capacity is independent of the confining condition, and by contrast, at low suctions (< 4MPa) the confined condition resulted in significant low water retention. Furthermore, the microstructure was investigated at Mercury Intrusion Porosimetry (MIP) and Environmental Scanning Electron Microscope (ESEM) in different states: on oven-dried powder, bentonite slurry, as-compacted and wetted samples. It has been observed that the soil powder is constituted of aggregates of various sizes; this aggregates are destroyed by fully saturation at a water content equal to the liquid limit; compaction at the initial water content of 11-12% and a dry density of 1.7 – 1.75 Mg/m^3 led to a microstructure characterized by an dense assembly of relatively well preserved aggregates; saturation of the compacted sample under constant volume condition defined a non-homogeneous microstructure with the presence of well preserved aggregates. This non-homogeneous microstructure would be due to the non uniform distribution of the generated swelling pressure within the soil sample upon wetting. The hydraulic conductivity determined has been found decreasing firstly and then increasing with suction decrease from the initial value of about 80 MPa to zero; the decrease can be attributed to the large pore clogging due to soft gel creation by exfoliation process, as observed at ESEM.

Keywords: GMZ bentonite, simultaneous profile method, infiltration cell, constant volume condition, hydraulic conductivity

1. Introduction

In the conception of the disposal of high-level radioactive waste at great depth, engineered barrier made of compacted bentonite is often considered to limit the transfer of water and radioactive matters below an acceptable level. As the bentonite is usually compacted at low water content, it is initially unsaturated and undergoes very high suctions; it is progressively wetted by water from the host formation. Because the wetting process is accompanied by the bentonite swelling, even without considering the thermal effect due to the heat emitted from the waste canister, the water transfer through the bentonite barrier is coupled to mechanical phenomena related to bentonite swelling. In addition, owing to the extremely large stiffness of the host formation (granite for instance), the bentonite wetting takes place in quasi constant volume condition. This shows the complexity of the problem.

Various works have been conducted on bentonites for engineered barrier. Dixon et al. (1987) performed permeability tests on bentonite Kunigel V1 of different mineralogy and evidenced a common relation between the dry density and the hydraulic conductivity at saturated state; this shows that the mineralogy is not a governing factor for the saturated hydraulic conductivity. Haug & Wong (1992) tested a bentonite at two densities, 1.67Mg/m^3 and 1.81Mg/m^3, with water content comprised between 6 and 19%; they showed that the initial water content did not affect the hydraulic conductivity at saturated state. Romero et al. (1999) studied the water permeability, water retention of compacted Boom clay; they interpreted the obtained results based on the mercury intrusion porosimetry (MIP) observations. Loiseau et al. (2002) determined the hydraulic conductivity of a heavily compacted bentonite-sand mixture (70% Kunigel V1 – 30% Hostun sand); they observed that in saturated condition, the permeability depends on the hydraulic gradient; in unsaturated condition, this dependence was found stronger because of the more significant interaction between clay and water. Hoffmann et al. (2007) studied the hydro-mechanical behavior of a bentonite pellet mixture, showing that the saturated hydraulic conductivity and the swelling pressure appeared to be mainly controlled by the overall dry density of the sample rather than the initial grain size distribution.

From a practical point of view, for a geological repository involving bentonite-based engineered barriers, the first question arisen is the time needed for the full saturation of bentonite barriers. Addressing this question requires a good understanding of the complex water transfer process within the barriers. Most of numerical methods developed for this purpose use the hydraulic conductivity-suction relationship. If this relationship has been relatively well studied for various reference bentonites as MX 80, Foca 7, Kunigel V1 etc. (see for instance Delage et al. 1998, Cui et al. 2008), it is not the case for the Chinese bentonite, Gao-Miao-Zi (GMZ) bentonite, which has been considered as a possible material for engineered barrier in the recent Chinese program of radioactive waste disposal at great depth. The present work deals with the hydraulic conductivity of this bentonite. Note that GMZ bentonite was selected for the Chinese program mainly according to its mineralogy composition and the quarry reserve.

2. Material

GMZ deposit is located in the northern Chinese Inner Mongolia autonomous region, 300 km northwest from Beijing. The deposit was formed in later Jurassic period. Bentonite is bedded, with a soapy texture and waxy appearance. The mineralization was a process of interaction between the firstly formed continental volcanic sediment and then suffering from interaction with ground water and weathering (Liu and Wen 2003).

Wen (2005) studied the mineralogy of GMZ bentonite. The analysis by X-ray diffraction shows that it is composed of 11.7% quartz, 7.3% cristobalite, 4.3% feldspar, 0.5% calcite, 0.8% kaolinite and 75.4% montmorillonite. It is mainly owing to its high montmorillonite content that this bentonite was selected for the geological disposal of high level radioactive wastes.

The bulk chemical component of GMZ bentonite was analyzed by X-ray fluorescence spectrometry: Al_2O_3 14.20%, SiO_2 67.43%, P_2O_5 0.02%, CaO 1.13%, K_2O 0.73%, TiO_2 0.12%, FeO 0.29%, TFe_2O_3 2.40%, MgO 0.10%, Na_2O 1.75%, MnO 0.02%, loss on ignition, 11.38%. The Cation Exchangeable Capacity (CEC) and exchangeable cations are presented in Table 1, and the main physical properties are listed in Table 2. The dominant cation is sodium (43.36 mmol/100g). The high CEC (77.3 mmol/100g) and the large specific surface (570 m^2/g) are in good agreement with a big plastic index (I_p = 275).

3. Experimental Methods

3.1. Instantaneous method

The unsaturated hydraulic conductivity was determined using the instantaneous profile method which needs the simultaneous monitoring of suction and volumetric water content profiles in a soil. The common practice is monitoring the suction profile only and the volumetric water content profile is deduced from the water retention curve determined separately (Daniel 1982); this method was adopted in the present work.

In the infiltration test performed by Daniel (1982), clay samples were hydrated by an end and the evolution of the relative humidity was followed using psychrometers at various positions. The suction profiles obtained, associated with the water retention curve, can be used to calculate the hydraulic conductivity as follows:

1) While measuring, at various positions in the sample, the value of suction at one moment t given, a suction profile can be plotted. The tangents to these profiles are calculated on each level x. They correspond to the hydraulic gradient i at the position x and the instant t.

$$i = \frac{ds}{dx} \tag{1}$$

where s is soil suction.

2) Based on the profiles of volumetric water content deduced from suction profiles and water retention curve, the water flux through a position x_i during a time

interval *Dt* can be calculated (Eq. 2).

$$q = A.\frac{\int_{X_i}^{L}(\theta)_{t+dt}.dx - \int_{X_i}^{L}(\theta)_{t}.dx}{\Delta t} \quad (2)$$

where *q* is water flux, *A* is the section of soil sample, *?* is volumetric water content, *x* is distance from the water source and L is the sample height.

3) By applying the generalized Darcy's law, hydraulic conductivity can be then determined using Eq 3.

$$k_w = -\frac{1}{A}.\frac{q}{\frac{1}{2}\left[i_t + i_{t+\Delta t}\right]} \quad (3)$$

where k_w is water hydraulic conductivity, i_t and i_{t+Dt} are hydraulic gradient at instant *t* and *t+Dt*, respectively.

3.2. Infiltration Test

The test infiltration was carried out on GMZ bentonite sample confined in a metallic column. During hydration the column prevented from any soil volume changes; this condition is close to that for a real storage in granite host rock. For the sample preparation, to ensure a total release of initial stress due to compaction, the soil was firstly statically compacted in a mould at the initial water content of 12.3% to reach a dimension of 150 mm high and 50 mm in diameter that corresponds to a dry density of 1.70 Mg/m^3. The compaction speed was 0.1 mm/min. In order to minimize the heterogeneity of the sample related to friction, the compaction was carried out in 5 layers.

After compaction, the sample was extruded from the mould. Because of the release of the confining stress it swelled slightly and its diameter was adjusted to 50 mm using a cutter. The final control showed that the sample density change due to the soil swell was negligible. The sample was then introduced in the infiltration cell by pushing. The two ends of the sample were confined by two stainless plates of 40 mm thick, encasing cylinder on both sides. The unit was maintained closed by 4 screws which could resist nominal swelling pressures up to 60 MPa. A porous stone was installed on the lower base as well as two valves for water infiltration. One valve was installed on the upper base plate for air escaping.

The suction measurement was made using resistive relative humidity transducers whose principle is based on the proportional variation of electrical intensity of a polymer with its humidity. Five transducers were installed every 30 mm, four on the cylinder and one on the upper base plate. As the used transducers measures the air humidity, no direct contact with soil sample was allowed. For this reason, a small cavity was bored in the soil for each transducer. This cavity had a dimension allowing introducing the transducer cap: a porous stone of 2 mm thick and 5 mm in diameter. This porous stone separated the transducer from the soil sample and allowed the air humidity transfer from the sample to the transducer. The schematic layout of the infiltration cell is presented in Figure 1 and a corresponding picture is shown in Figure 2.

After installation of the sample, several weeks were waited for suction homogenization in the sample. Then, water infiltration was started through valve (R1).

3.3. Determination of water retention curve

To apply the simultaneous method, the water retention curve must be determined under the same condition as for the monitoring of suction profile, i.e., under constant volume condition. In this study, both water retention curves of GMZ bentonite under confined and unconfined conditions were determined, using vapor equilibrium technique (high suction range) and osmotic technique (low suction range); the curve under confined condition will be used for hydraulic conductivity determination and the curve under unconfined condition was used for comparison. To ensure the constant volume condition, a special stainless steel cell was designed with two perforated ends. The dimension of the cell is 6 mm high and 20 mm in diameter. As for the infiltration test, the soil samples were compacted in a separate mould to a dry density of 1.70 Mg/m^3, adjusted if necessary and then introduced in the cell.

To apply the vapor equilibrium technique, the cell was placed in a desiccator contained saturated salt solution (Delage et al. 1998; Saiyouri et al. 2000; Montes-H et al. 2003, Tang et Cui 2005). The test was carried out in an air-conditioned room with temperature controlled at 25±1°C. The salts used and the corresponding suction are presented in Table 3. The sample was initially brought to 309 MPa suction using $LiCl.H_2O$ solution then progressively wetted to 113 MPa (K_2CO_3), 82 MPa ($MgNO_3$), 57 MPa ($NaNO_2$), 38 MPa (NaCl), 24.9 MPa ($(NH_4)_2SO_4$), 12.6 MPa ($ZnSO_4$), 9 MPa (KNO_3) and 4.2 MPa (K_2SO_4). The water content at equilibrium under each suction was determined by weighing.

As far as the unconfined condition is concerned, the soil sample was compacted to a dry density of 1.70 Mg/m^3, extruded from the mould and placed in the desiccator containing saturated salt solution. The same drying-wetting path was followed.

To apply the osmotic technique (Delage and Cui 2008) under confined condition, semi-permeable membrane was placed between the perforated ends and the soil sample. The cell was then placed in PEG solution of a given concentration. Water transfer occurred through the small holes and the semi-permeable membrane. In practice, the PEG concentration was controlled by Brix index (Delage et al. 1998) using a refractometer. Three suctions (0.013, 0.099 and 0.736 MPa) were considered and the correspondence between Brix index and suction is presented in Table 4. The water content at equilibrium under each suction was determined by weighing.

For unconfined condition, the sample was wrapped in the semi-permeable membrane and then immersed in the PEG solution. The same suctions were applied.

3.4. Microstructure observations

Mercury Intrusion Test was performed on as-compacted and wetted samples. The two samples were compacted statically at a water content of 11.1% to reach a density of 1.75 Mg/m^3. For the as-compacted sample, after compaction, thin soil slices were taken by cutting from the sample and then lyophilized by freeze-drying (Sridharan et

al. 1971, Delage and Pellerin 1984). For the wetted sample, after compaction, it is introduced in a cell (20 mm high and 50 mm in diameter) to undergo constant-volume saturation. The sample was then taken from the cell, and as for the as-compacted sample thin soil slices were taken from it for lyophilizing by freeze-drying. The conditions of the two samples prior to freeze-drying are presented in Table 5. It can be observed that the water content increased from 11.1% to 24.4% after saturation and that the dry density decreased from 1.75 Mg/m^3 to 1.65 Mg/m^3. The density decrease was mainly due to the swelling pressure release when the sample was taken from the saturation cell.

Environmental Scanning Electron Microscope (ESEM) was used for microstructure observation; the primary advantage of this technique compared to conventional Scanning Electron Microscope (SEM) being that the ESEM does not require the soil sample to be initially lyophilized (Deohne and Stulik 1990). Four samples were observed at ESEM: powder, slurry, as-compacted and wetted samples. The slurry was prepared by adding distilled water to reach a water content as high as the liquid limit (313%); the as-compacted and wetted samples were prepared as indicated above. The conditions of the samples are listed in Table 6.

4. Experimental Results

4.1. Hydraulic conductivity

The data obtained with the vapor equilibrium technique and osmotic technique are gathered to determine the water retention curves (Figure 3). It is observed that at suctions higher than 4 MPa, the water retention curves under confined and unconfined conditions are almost the same. However, at suctions lower than 4 MPa, the confined condition gave much lower water content: under near zero suction (0.013 MPa) the difference in water content is as large as 140%. The same phenomenon was observed by Yahia-Aissa et al. (2001) on French FoCa 7 clay and Cui et al. (2008) on a mixture (7/3 by weight) of Kunigel V1 bentonite and Hostun sand. Indeed, for Foca 7 clay, the water retention curve shows a difference between confined and unconfined condition when the suction is lower than 3-4 MPa; for the mixture of Kunigel V1 bentonite / Hostun sand, this threshold suction is 4-5 MPa.

Figure 4 presents the evolution of the relative humidity (RH) recorded by the humidity sensors during the infiltration test. The curves are well ordered as a function of the distance from the infiltration source: at 30 mm position only 600 hours were needed to reach 90% relative humidity; 3600 hours were needed to reach the same relative humidity at 60 mm position; much more time was needed for other more distant positions. To convert the relative humidity to suction, Kelvin's law was used:

$$s = -\left(\frac{R.T}{g.M}\right) LnRH \qquad (4)$$

where R is the constant for perfect gas (8.314 J mol^{-1}K^{-1}), T is absolute temperature (K), RH is relative humidity. Figure 5 shows the evolution of suction during the

infiltration.

The suction profiles for every 200 hours are determined and showed in Figure 6. As it can been seen, the initial suction of the sample was quite homogeneous, around 80 MPa.

The hydraulic gradients are deduced from the tangents to the profiles of hydraulic head which is deduced from the suction profiles (Figure 7) and the water fluxes are calculated starting from the profiles of volumetric water content integrated two to two (Figure 8).

The variation of hydraulic conductivity with suction was determined using equation 3 and is presented in Figure 9. When the suction was reduced from the initial value of about 80 MPa to zero, the hydraulic conductivity of GMZ bentonite was firstly decreasing (70 MPa = s = 80 MPa) then increasing with suction decrease (0 = s < 70 MPa). The hydraulic conductivity is about 2 x 10^{-14} m/s at 80 MPa suction, 7 x 10^{-15} m/s at 70 MPa suction. At zero suction the value is about 10 x 10^{-13} m/s which is similar to that from number of published tests on similar materials. Indeed, Kröhn (2003) gathered the permeability data obtained on MX 80 bentonite by several authors (Pusch 1980a, b; Bucher and Spiegel 1984; Pusch et al. 1990, 1999; Börgesson et al. 1995, 1996; Rodwell et al. (1999); Karnland et al. (2000); Pusch and Swemar 2000; all in Kröhn 2003), and found that the permeability decreased with dry density in the linear fashion and that at a dry density of 1.7 Mg/m^3 (the value considered in this study) the hydraulic conductivity was comprised between 2 x 10^{-14} and 2 x 10^{-13} m/s.

4.2. Microstructure Investigation

Figure 10 presents the Pore Size Distribution (PSD) curves (cumulated – Figure 10a; derived – Figure 10b) from the MIP tests. Only one family between 0.1 and 2 µm was clearly identified for both as-compacted and wetted samples. Comparison between the total porosities identified by MIP and that deduced from the densities of the big samples shows a difference of 0.021 cm^3/g for as-compacted sample (0.18 against 0.201) and 0.081 cm^3/g for wetted sample (0.155 against 0.236). This difference, especially for wetted sample, evidences that a significant quantity of micro-pores (smaller than 0.1 µm) was not identified by MIP. This feature is similar to that observed on compacted bentonite samples (Delage et al. 2006).

Figure 11 presents the ESEM photos of GMZ bentonite in powder form (Figure 11a) and slurry form (Figure 11b), respectively. It can be observed that the bentonite powder corresponds to an assembly of aggregates of various sizes, the biggest reaching about 50 µm in diameter. In slurry form, the aggregates can be no longer observed: the full hydration destroyed the aggregates, giving rise to a relatively homogenous bee-nest structure.

Figure 12 presents the ESEM photos of as-compacted sample (Figure 12a) and wetted sample (Figure 12a), respectively. The microstructure of as-compacted sample, compared to that of powder, is a denser assembly of clay aggregates. The overall structure is homogeneous with no clear big inter-aggregates pores. For the wetted sample, the leaf-like microstructure evidences the effect of hydration. The hydration seems to be however not homogenous: unlike for the slurry, well preserved aggregates

can be observed in the wetted sample. The long pores observed in the right part are probably due to the swelling pressure release.

5. Discussion

The PSD curves from MIP tests evidenced one predominant pore family between 0.1 and 2 µm for both as-compacted and wetted samples (Figure 10). This is consistent with the observation made at ESEM: only small pore between aggregates were observed (Figure 12), the aggregates being similar to that identified on oven-dried powder (Figure 11a).

Comparison between the PSD curve of as-compacted sample and that of wetted sample showed that the difference between the total porosity from big sample and that from MIP test is much more significant in case of wetted sample; in addition, the PSD curve of wetted sample is beneath that of as-compacted sample. This shows that the quantity of pores non identifiable by MIP tests was significantly increased by the saturation process under constant volume condition. In fact, when water infiltrated into the soil it can be assumed that big pores were first filled with water in either liquid or vapor form and then the clay aggregates hydration started. The aggregates hydration led to the exfoliation phenomenon corresponding to the separation of the clays sheets, creating a soft clay gel (Cui et al. 2002, Kröhn 2003, Pusch and Yong 2006). In case of unconfined condition, this separation process could fully develop with large quantity of water inserted between clay sheets. By contrast, in case of confined condition the separation process could not fully develop because of the generated swelling pressure that limited the water adsorption into the interlayer space and thus the separation of clay sheets. Moreover, under confined condition the distribution of swelling pressure in the soil sample seemed to be not uniform since the swelling of individual aggregates was found different: well preserved aggregates were identified at ESEM (Figure 12b).

Comparison between the water retention curve of confined sample and that of unconfined sample showed that under high suctions ($s > 4$ MPa) the two curves are almost the same, and that under lower suctions ($s < 4$ MPa) the curve of confined sample is much lower than that of unconfined sample (Figure 3). The lower water content at zero suction in case of confined condition is consistent with the microstructure observation mentioned above; the independency of the water retention curve on the hydration condition at high suctions shows that in the beginning of wetting, aggregates hydration resulted in filling large pores by clay sheet exfoliation (Cui et al. 2002, Kröhn 2003, Pusch and Yong 2006). This process having taken place microscopically in the macro-pores and therefore under unconfined or near unconfined condition, independent of overall confining condition. Obviously, this process corresponds to a homogenisation of the microstructure. When the exfoliation phenomenon ended, the initial macro-pores were filled with soft clay gel. Further water uptake must correspond to the water adsorption into the interlayer space of clay particles. This adsorption can fully develop in the case of unconfined condition with significant clay swelling. But it is not the case under confined condition with swelling

prevented. As a result, for same suction the water content is lower under confined condition.

As far as the hydraulic conductivity is concerned, it was observed that suction decrease resulted in firstly a decrease then an increase of hydraulic conductivity (Figure 9). This result does not correspond to the observation commonly made on non-expansive unsaturated soils, for which hydraulic conductivity increases in a continuous way upon wetting. In fact, as deduced from the MIP and SEM observations and in agreement with the conclusions by Cui et al. (2002), Kröhn (2003), Pusch and Yong (2006), water infiltration under confined condition leads to bentonite aggregates hydration and exfoliation phenomenon occurs around the macro-pores, giving rise to the creation of a soft gel. As in the beginning water transfer is primarily governed by the network of large pores and these large pores are progressively decreasing in quantity and in size due to the gel creation (see Figure 12), the hydraulic conductivity decreases. After completion of this large-pore clogging by gel creation, water transfer is only governed by the suction gradient and thus common hydraulic conductivity evolution can be observed.

It should be mentioned that the bentonite hydration in the infiltration test is a diffusion-controlled process rather than a convection-controlled process, as described by Kröhn (2003) and Pusch and Yong (2006). Furthermore, water vapor diffusion prevails in the zone little far from the wetting face. Indeed, Delage et al. (1998) performed infiltration tests on both the pure Kunigel VI bentonite (at an overall dry density of 18 Mg/m^3) and the mixture of Kunigel V1 bentonite/Hustun sand (7/3 by weight, at an overall dry density of 2.03 Mg/m^3) under confined condition, and they observed an almost vertical suction profiles in all time when the distance from the wetting face was far than 50 mm. As the suction was deduced from the measured total relative humidity, they concluded that within the part beyond 50 mm far from the wetting surface the water transfer was mainly governed by vapor diffusion. Examination of Figure 6 shows that in the case of GMZ bentonite compacted to an overall dry density of 1.7 Mg/m^3, the suction profiles are less vertical, showing a relatively less prevailing vapor transfer. This is probably related to its lower overall dry density (1.7 against 1.8 or 2.03 Mg/m^3).

As the microstructure, which largely determines the hydraulic conductivity, undergoes transient changes in the course of infiltration, the determined hydraulic conductivity is microstructure dependant. This is particularly the case during the exfoliation process. Therefore, the infiltration test performed should be regarded as a small scale mock-up test. However, it is believed that the conductivity-suction relationship determined is relevant when the exfoliation process ended, i.e. when the suction was lower than about 70 MPa. Furthermore, as most numerical assessment methods for water transfer have not accounted for the effect of gel creation by exfoliation, it seems that the obtained conductivity-suction relationship allows implicit consideration of the gel creating by using parameters derived from this experimental relationship.

6. Conclusions

GMZ bentonite has been considered as a possible material for engineered barrier in the Chinese program of geological nuclear waste disposal. The hydraulic conductivity of this bentonite was determined using simultaneous profile method; the suction profiles were determined using an infiltration cell equipped with five resistive relative humidity probes, and the water content profiles were deduced from the water retention curve which was determined under confined condition. Furthermore, the water retention curve at unconfined condition was also determined for comparison. The microstructure was investigated at MIP and ESEM in different conditions: on oven-dried powder, bentonite slurry, as-compacted and wetted samples. The following conclusions can be drawn.

When compacted GMZ bentonite at its initial water content of about 11 – 12% and a dry density of about 1.7 Mg/m^3, only one predominant pore family was identified corresponding to the pores between aggregates. This observation is consistent with that at ESEM.

As compared to unconfined sample, the quantity of pores non identifiable by MIP test was significantly increased for confined sample, showing the large-pore clogging phenomenon in the confined sample upon wetting. This phenomenon occurred at high suctions ($s > 4$ MPa) and during clogging there is equivalence of overall confined swelling to unconfined swelling.

When soil suction was decreased from the initial value (about 80 MPa) to zero, the hydraulic conductivity firstly decreased from 2 x 10-14 m/s to 7 x 10-15 m/s and then increased to 10 x 10-13 m/s which is the value at saturated state. The conductivity decrease with suction decrease is related to the soft gel created by exfoliation process that occurs around the macro-pores during aggregates hydration. Indeed, as in the beginning water transfer is primarily governed by the network of large pores and these large pores are progressively decreasing in quantity and in size, the hydraulic conductivity decreases. After completion of this large-pore clogging by gel creation, a normal conductivity increase with suction decrease was observed.

The bentonite hydration in the infiltration test is a diffusion-controlled process rather than a convection process. Furthermore, water vapor diffusion prevails in the zone little far from the wetting face. Comparison of suction profiles between GMZ bentonite sample and Kunigel V1 bentonite sample or Kunigel V1/Hostun sand mixture sample showed that the water vapor diffusion is dry density dependent: the higher the overall dry density, the larger the water vapor diffusion.

The conductivity evaluated has been found to be microstructure dependent. It is however believed that the conductivity-suction relationship determined is relevant when the exfoliation process ended, i.e. when the suction was lower than about 70 MPa for GMZ bentonite. Furthermore, from a practical point of view, it seems that the obtained conductivity-suction relationship allows implicit consideration of the gel creating when assessing water transfer pragmatically using most numerical models provided that the used parameters are derived from this experimental relationship.

7. Acknowledgments

The authors are grateful to the National Natural Science Foundation of China for the financial supports (No. 40572161; No.40728003; No.40772180).

8. References

Börgesson L., Johannesson L.-E., Sanden T., Hernelind J., 1995. Modelling of the physical behaviour of water saturated clay barriers. SKB Technical Report TR-95-20.

Börgesson L., Karnland O., Johannesson L.-E., 1996. Modelling of the physical behaviour of clay barriers close to water saturation. Engineering Geology 41, 127–144.

Bucher F., Spiegel U., 1984. Quelldruck von hochverdichteten Bentoniten. Nagra Technical Report NTB 84-18.

Cui Y.J., Loiseau C., Delage P., 2002. Microstructure changes of a confined swelling soil due to suction controlled hydration, In: Proc 3rd Int Conf on Unsaturated Soils, UNSAT'2002 Recife, Brazil, Balkema 2, 593-598.

Cui Y.J., Tang A.M., Loiseau C. & Delage P., 2008. Determining water permeability of compacted bentonite-sand mixture under confined and free-swell conditions. Physics and Chemistry of the Earth, 33, S462-S471.

Daniel D. E.,1982. Measurement of Hydraulic Conductivity of Unsaturated Soils with Thermocouple Psychrometers. Soil Science Society of America Journal, Vol. 46, n°6, 1125-1129.

Delage P., Lefebvre G., 1984. Study of the structure of a sensitive Champlain clay and its evolution during consolidation, Can Geotech J 21(1), 21-35.

Delage P., Cui Y.J., Yahia-Aissa M., De Laure E., 1998. On the unsaturated hydraulic conductivity of a dense compacted bentonite. Proc. of Unsat'98, Beijing, vol. 1, 344-349.

Delage P., Howat M., Cui Y.J., 1998. The relationship between suction and swelling properties in a heavily compacted unsaturated clay, Eng Geology 50(1-2), 31-48.

Delage P., Cui Y.J., 2008. An evaluation of the osmotic method of controlling suction. Geomechanics and Geoengineering: An International Journal, 3(1), 1-11.

Delage P., Marcial D., Cui Y. J., Ruiz X., 2006. Ageing effects in a compacted bentonite: a microstructure approach. Géotechnique, 56, No. 5, 291–304.

Dixon D.A., Cheung S.C.H., Gray M.N., Davidson B.C., 1987. The hydraulic conductivity of dense clay soils, In: Proc. 40th Canadian Geotechnical Conference, Regina, Saskachewan - Canada, 389-396.

Doehne E., Stulik D.C., 1990. Applications of the environmental scanning electron microscope to conservation science. Scanning Microscopy, 4, 275-286.

Haug M.D., Wong L.C., 1992. Impact of molding water content on hydraulic conductivity of compacted sand-Bentonite, Can Geotech J, 29, 253-262.

Hoffmann C., Alonso E.E., Romero E., 2007. Hydro-mechanical behaviour of bentonite pellet mixtures, Physics and Chemistry of the Earth 32, 832-849.

Karnland O., Sanden T., Johannesson L.-E., Eriksen T.E., Jansson M., Wold S., Pedersen K., Motamedi M., Rosborg B., 2000. Long term test of buffer material, Final report on the pilot parcels. SKB Technical Report TR-00-22.

Kröhn K.-P., 2003. New conceptual models for the resaturation of bentonite. Applied Clay Science 23 (1–4), 25–33.

Liu Y.M., Wen Z.J., 2003. An investigation of the physical properties of clayey materials used in nuclear waste disposal at great depth. Mineral Rocks, vol. 23 (4), 42-45, in Chinese.

Loiseau C., Cui Y.J., Delage P., 2002. The gradient effect on the water flow through a compacted swelling soil, In: Proc. 3rd Int Conf Unsaturated Soils, UNSAT'2002 Recife, Brazil, Balkema 1, 395-400

Montes-H G., Duplay J., Martinez L., Mendoza C., 2003. Swelling-schrinkage kinetics of MX80 bentontie, Applied Clay Science 22, 279-293.

Pusch R., 1980a. Water uptake, migration and swelling characteristics of unsaturated and saturated, highly compacted bentonite. SKBF/KBS Technical Report 80-11.

Pusch R., 1980b. Permeability of high compacted bentonite. SKBF/KBS Technical Report 80-16.

Pusch R., Karnland O., Hökmark H., 1990. GMM—a general microstructural model for quantitative studies of smectite clays. SKB Technical Report TR-90-43.

Pusch R., Muurinen A., Lehikoinen J., Bors J., Erikson T., 1999. Microstructural and chemical parameters of bentonite as determinants of waste isolation efficiency. European Comission Report EUR 18950 EN.

Pusch R., Svemar Ch., 2000. Prototype Repository Project: WP3 Modelling Meeting. Minutes of the Meeting in Lund. SKB, Stockholm.

Pusch R., and Yong R., 2006. Microstructure of smectite clays and engineering performance, Taylor & Francis, 328p.

Rodwell W.R., Harris A.W., Horseman S.T., Lalieux P., Müller W., Ortiz Amaya L., Pruess K., 1999. Gas migration and twophase flow through engineered and geological barriers for a deep repository for radioactive waste. Joint EC/NEA Status Report EUR 19122.

Romero E., Gens A., Lloret A., 1999. Water permeability, water retention and microstructure of unsaturated compacted Boom clay, Eng Geology 54, 117-127.

Saiyouri N., Hicher P.Y., Tessier D., 2000. Microstructural approach and transfer water modeling in highly compacted unsaturated swelling clays, Mech Cohesive Frictional Mater 5, 41-60.

Sridharan A., Altschaeffl A.G., Diamond S., 1971. Pore size distribution studies. Journal of Soil Mechanics and Foundation Engineering, 97, (SM 5), 771–787.

Tang A.M., Cui Y.J., 2005. Controlling suction by the vapour equilibrium technique at different temperatures and its application in determining the waer retention properties of MX 80 clay, Can Geotech J 42, 1-10.

Wen Z.J., 2005. The selection and the basic properties of a engineered barrier material used in the geological disposal of high level radioactive waste in China, vol. 24 (6): 583-586, in Chinese.

Yahia-Aissa M., Delage P., Cui Y.J., 2001. In: Adachi, Fukue (eds) Suction-water

relationship in swelling clays, Clay Science for Engineering, IS-Shizuoka Int Symp on Suction, Swelling, Permeability and Structure of Clays, Balkema, 65-68.

Table 1 CEC and exchangeable cation of GMZ bentonite

Sample	CEC (mmol/100g)	Exchangeable cation (mmol/100g)				Alkali Index
		$E(k^+)$	$E(Na^+)$	$E(1/2Ca^{2+})$	$E(1/2Mg^{2+})$	
GMZ	77.30	2.51	43.36	29.14	12.33	1.14

Table 2 Main physical properties of GMZ bentonite

Sample	G_s	w_L(%)	w_P(%)	I_p	S (m^2/g)
GMZ	2.66	313	38	275	570

Table 3. Salts used and the corresponding suctions

Salt	Suction/MPa
K_2SO_4	4.2
KNO_3	9.0
$ZnSO_4$	12.6
$(NH_4)_2SO_4$	24.9
NaCl	38.0
$NaNO_2$	57.0
$MgNO_3$	82.0
K_2CO_3	113.0
$LiCl.H_2O$	309.0

Table 4. PEG solutions used and the corresponding suctions

Brix (%)	Suction (MPa)
18.5	0.736
7.8	0.099
3.0	0.013

Table 5. The conditions of the samples

Sample	Initial dry density (Mg/m^3)	Water content (%)	Void ratio
As-compacted	1.75	11.1	0.55
Wetted	1.65	24.4	0.64

Table 6. Initial conditions of the samples tested in ESEM

Sample	Water content (%)	Dry density (Mg/m^3)	Remarks
1	11.1		Powder
2	313		Slurry
3	11.1	1.75	Statically compacted
4	24.4	1.65	Statically compacted; saturated under constant volume condition

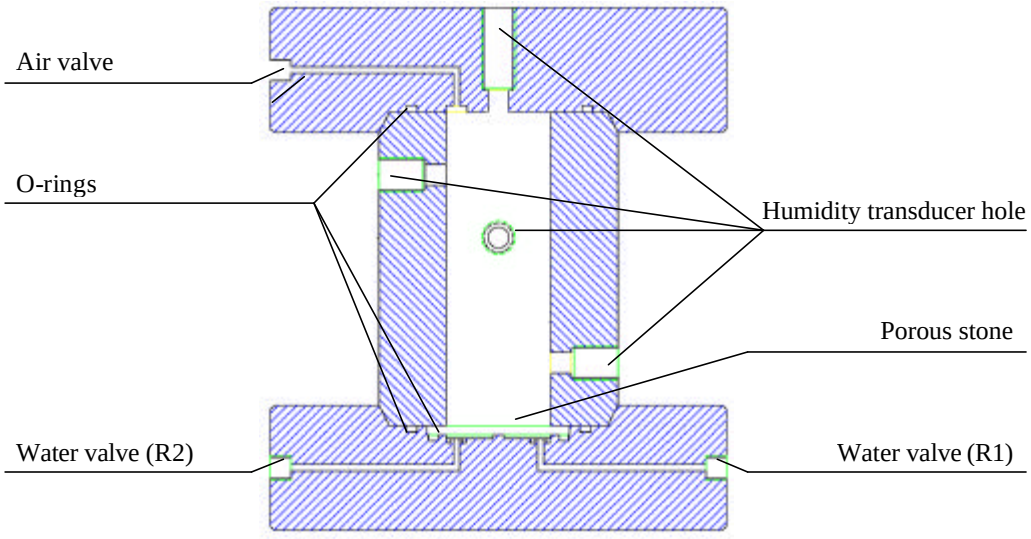

Figure 1. Schematic layout of the infiltration cell

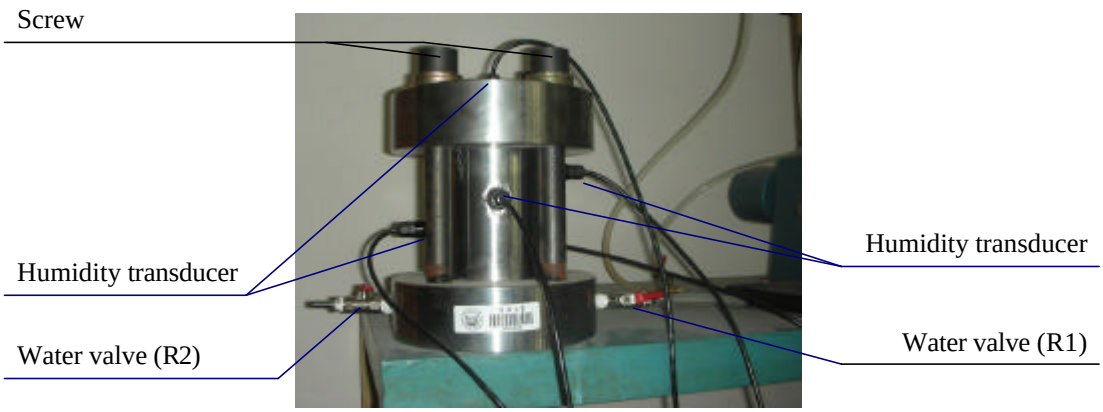

Figure 2. Setup of infiltration test on GMZ bentonite

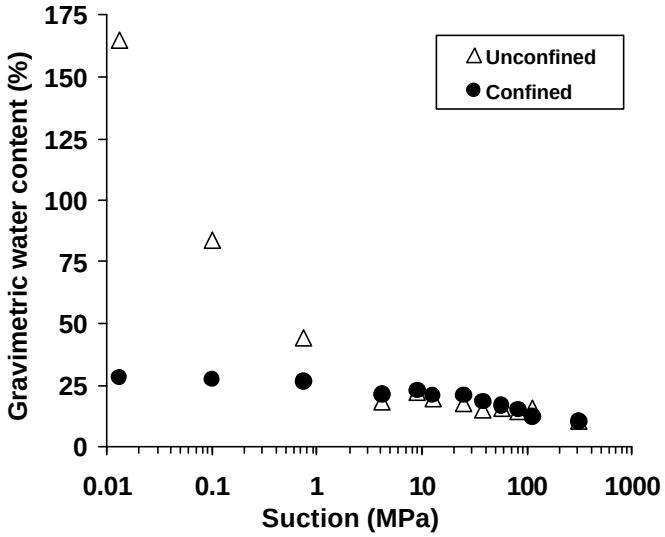

Figure 3. Water retention curves of GMZ bentonite

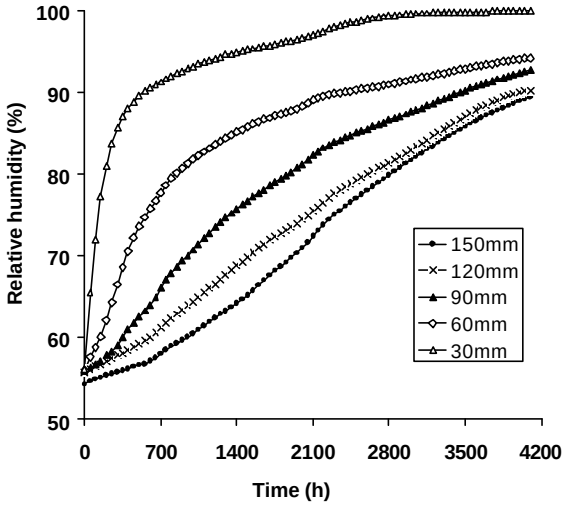

Figure 4 Hydration of the GMZ bentonite sample

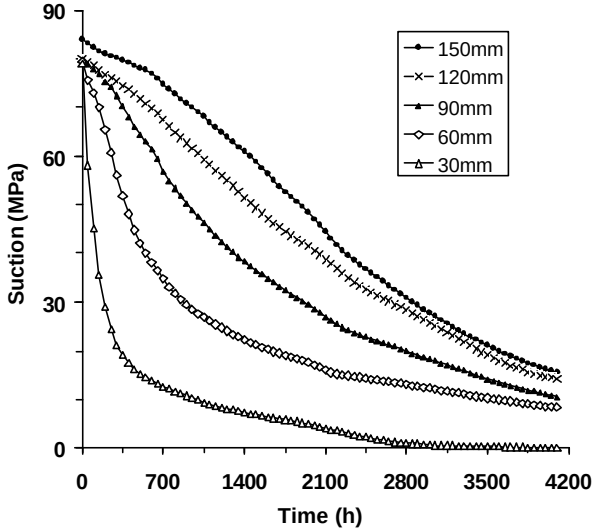

Figure 5. Evolution of suction during infiltration

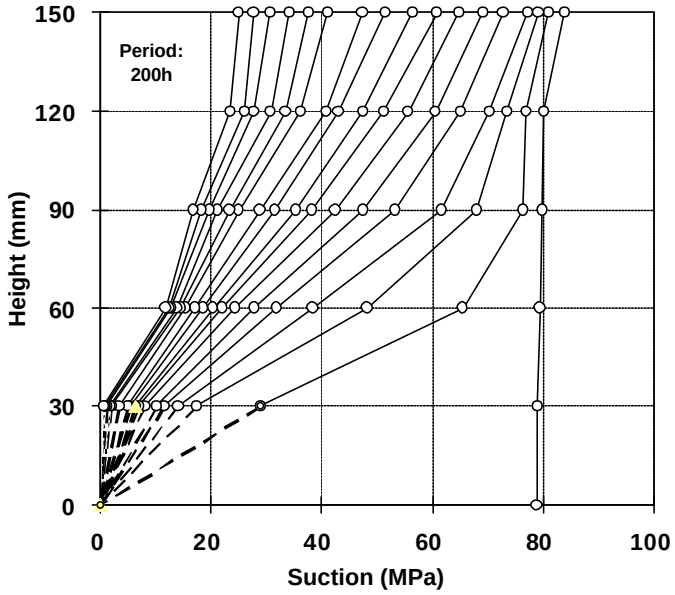

Figure 6. Suction profiles

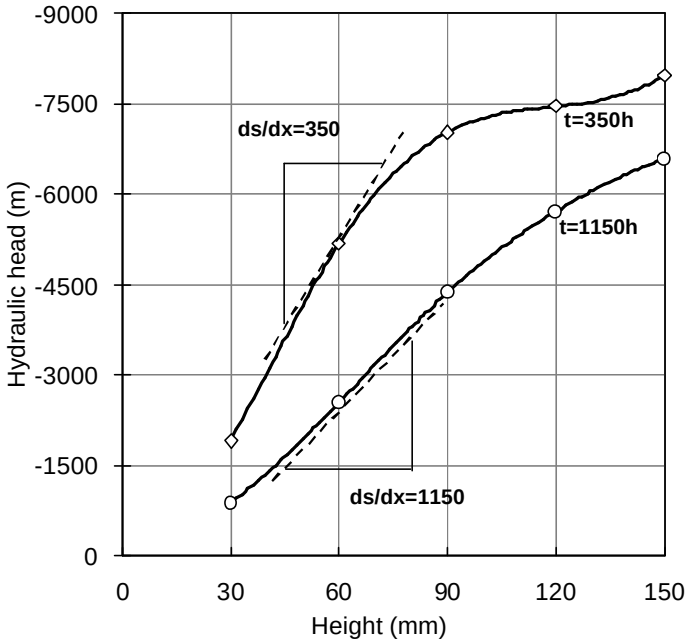

Figure 7. Determination of hydraulic gradient

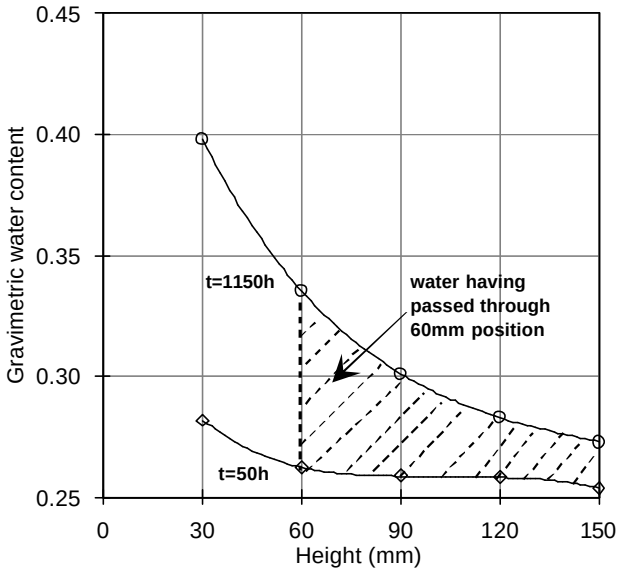

Figure 8. Determination of water flux

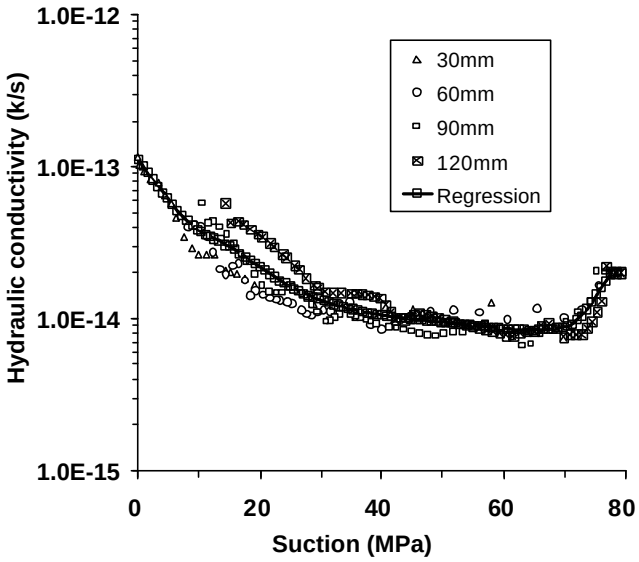

Figure 9. Variation of hydraulic conductivity of GMZ bentonite with suction

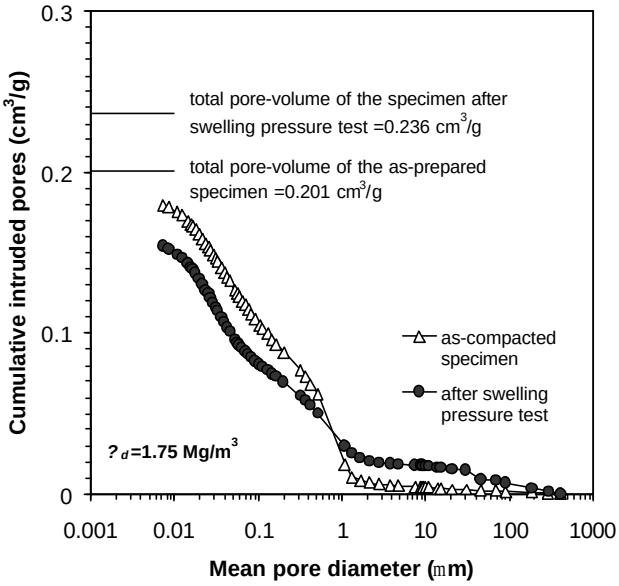

(a)

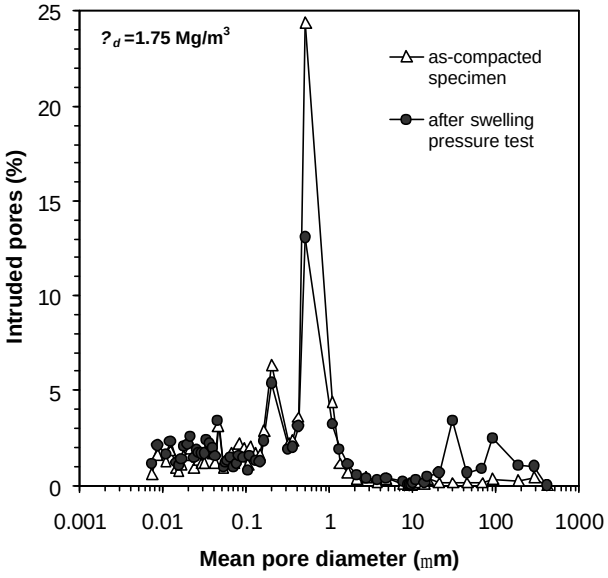

(b)

Figure 10. Pore-size distribution of as-compacted and wetted Compacted GMZ bentonite; a) cumulated curve (b) derived curve

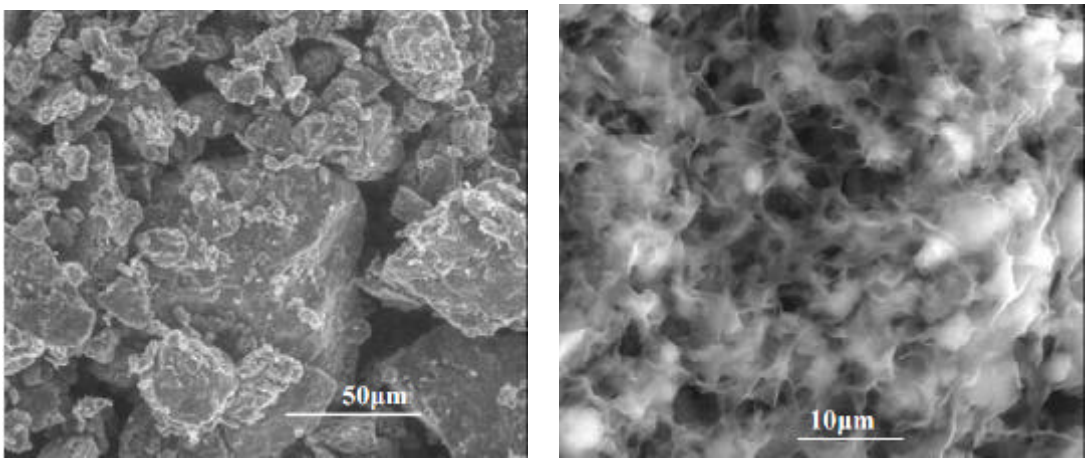

(a) (b)

Figure 11. ESEM photos of GMZ bentonite: (a) Sample 1 (powder); (b) Sample 2 (slurry)

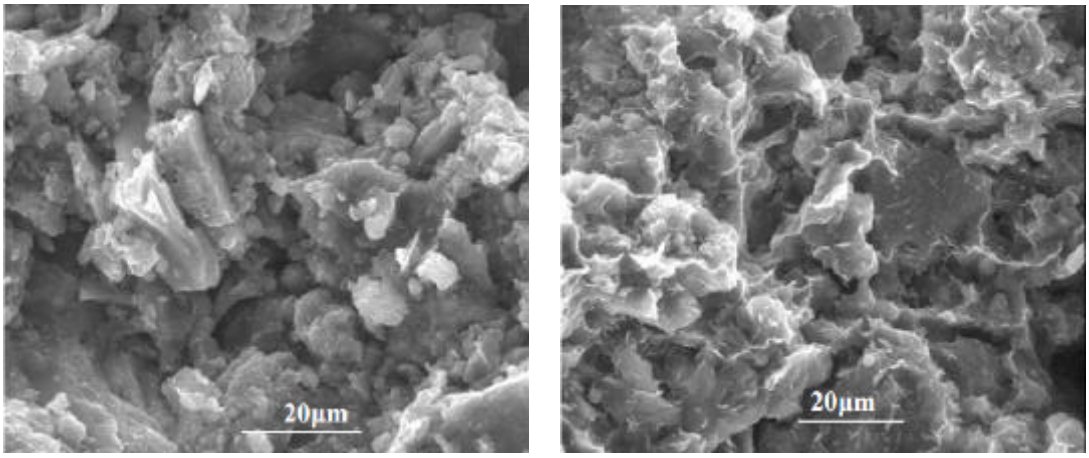

(a) (b)

Figure 12. ESEM photos of GMZ bentonite: (a) Sample 3 (as-compacted, dry density 1.75 Mg/m^3); (b) Sample 4 (wetted, dry density 1.65 Mg/m^3)